CONF-950793--48

UCRL-JC- 121619
PREPRINT

Performance of laser guide star adaptive optics at Lick Observatory

Scot S. Olivier, Jong An, Kenneth Avicola, Horst D. Bissinger,
James M. Brase, Herbert W. Friedman, Donald T. Gavel, Claire E. Max,
J. Thaddeus Salmon, Kenneth E. Waltjen

This paper was prepared for submission to the
SPIE '95 International Society for Optical Engineering
Adaptive Optical Systems and Applications
July 10-11, 1995, San Diego, CA

July 19, 1995

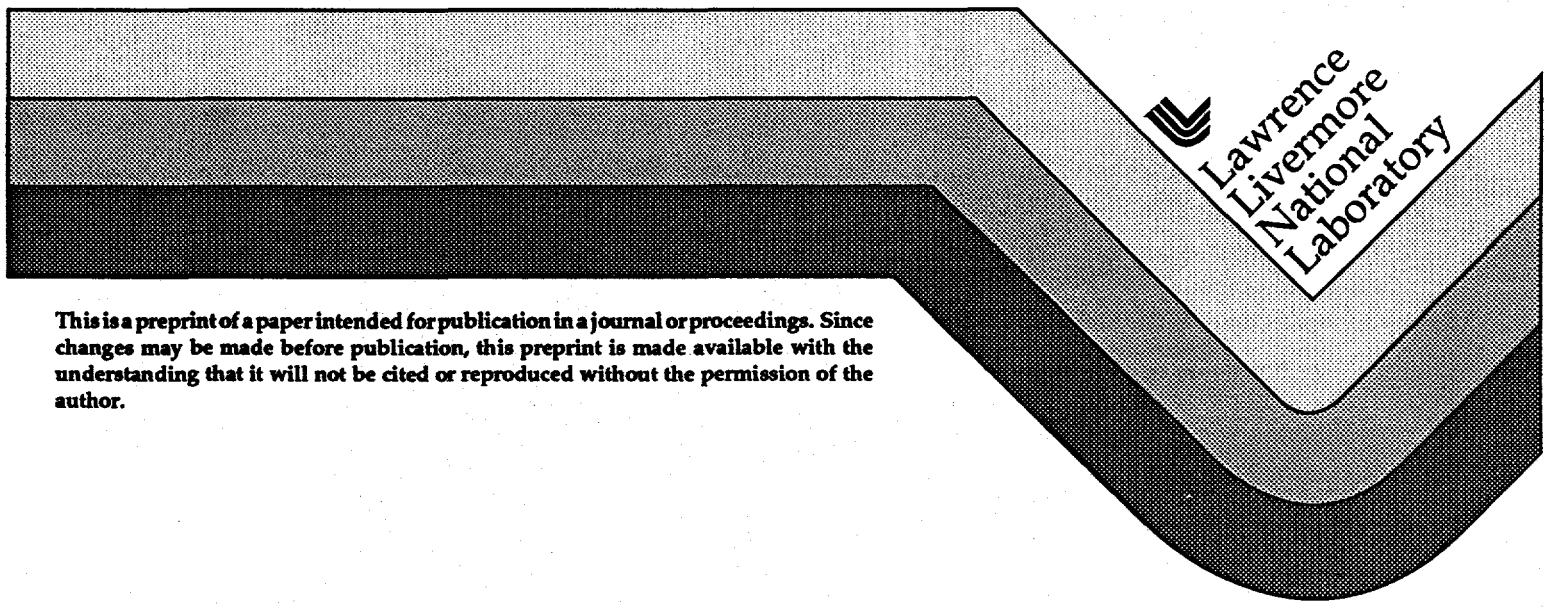

DISCLAIMER

Portions of this document may be illegible in electronic image products. Images are produced from the best available original document.

Performance of laser guide star adaptive optics at Lick Observatory

Scot S. Olivier, Jong An, Kenneth Avicola, Horst D. Bissinger,
James M. Brase, Herbert W. Friedman, Donald T. Gavel,
Claire E. Max, J. Thaddeus Salmon, Kenneth E. Waltjen

Lawrence Livermore National Laboratory, Livermore, CA 94550.

ABSTRACT

A sodium-layer laser guide star adaptive optics system has been developed at Lawrence Livermore National Laboratory (LLNL) for use on the 3-meter Shane telescope at Lick Observatory. The system is based on a 127-actuator continuous-surface deformable mirror, a Hartmann wavefront sensor equipped with a fast-framing low-noise CCD camera, and a pulsed solid-state-pumped dye laser tuned to the atomic sodium resonance line at 589 nm.

The adaptive optics system has been tested on the Shane telescope using natural reference stars yielding up to a factor of 12 increase in image peak intensity and a factor of 6.5 reduction in image full width at half maximum (FWHM). The results are consistent with theoretical expectations. The laser guide star system has been installed and operated on the Shane telescope yielding a beam with 22 W average power at 589 nm. Based on experimental data, this laser should generate an 8th magnitude guide star at this site, and the integrated laser guide star adaptive optics system should produce images with Strehl ratios of 0.4 at 2.2 μm in median seeing and 0.7 at 2.2 μm in good seeing.

1. INTRODUCTION

The resolution of astronomical images obtained from the ground is limited to angular sizes much greater than the theoretical diffraction limit of large telescopes by aberrations associated with atmospheric turbulence. In 1953, Babcock[1] suggested that these aberrations could be sensed and corrected in real time using an adaptive optics system thereby producing diffraction-limited images. In 1982, Happer et al.[2] proposed that a reference source for an adaptive optics system could be generated anywhere in the sky by resonant scattering of 589 nm light from the mesospheric sodium layer at ~100 km altitude. These concepts are now being applied by a number of groups to improve astronomical images[3].

A sodium-layer laser guide star adaptive optics system has been developed at LLNL for use on the 3-meter Shane telescope at Lick Observatory. A picture of the system on the telescope is shown in Figure 1. The adaptive optics system has been tested on the Shane telescope using natural reference stars, and the laser guide star system has been installed and operated on the telescope.

In this paper, we will describe the laser guide star adaptive optics system and present results from the engineering tests of the subsystems. The test results will be compared with theory, and will be used to predict the performance of the integrated system.

2. SYSTEM DESCRIPTION

2.1 Adaptive Optics System

The Lick adaptive optics system uses a Hartmann wavefront sensor, currently configured with a triangular array of 37 subapertures in the clear aperture of the telescope. The subapertures have a diameter of 46 cm mapped onto the telescope primary aperture. Images from the lenslets are recorded using a high-quantum-efficiency low-noise fast CCD camera built for LLNL by Adaptive Optics Associates using a 64 × 64 chip developed by Lincoln Laboratory.

The wavefront tilt data recorded by the wavefront sensor are used to reconstruct the wavefront phase. The wavefront reconstructor is based on four Intel i860 chips on a Mercury VME board and is controlled by a Unix workstation. The details of the real-time control system have been described in a previous paper[4].

The reconstructed wavefront phase is used to control a deformable mirror developed and built at LLNL with a triangular array of 127 electrostrictive lead magnesium niobate (PMN) actuators. These actuators have

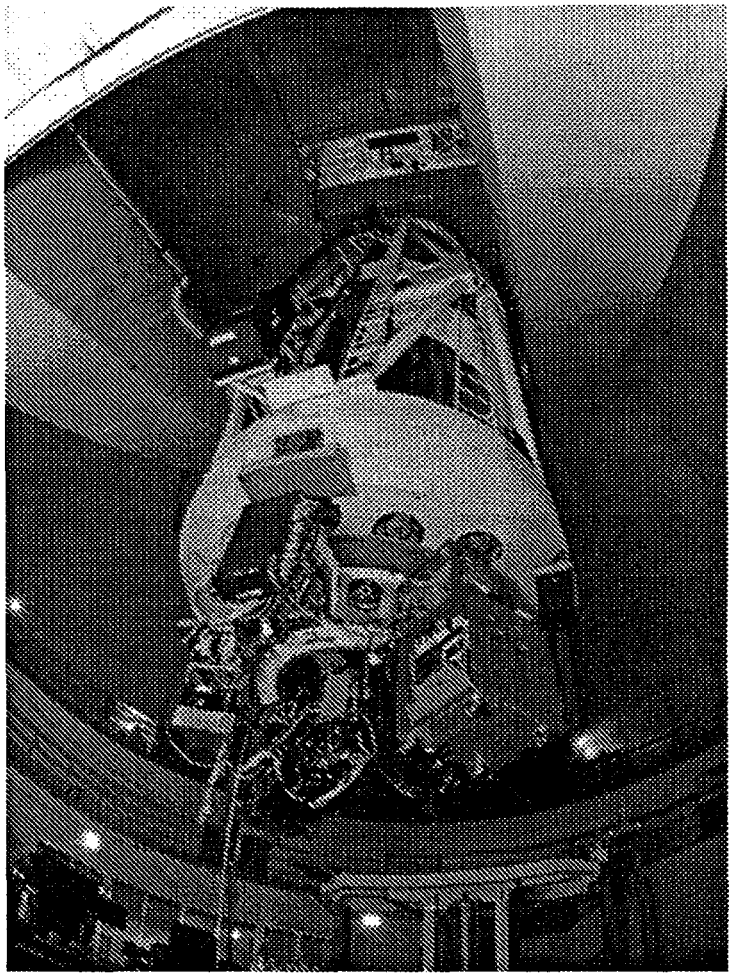

Figure 1 – Laser guide star adaptive optics system on the 3-meter Shane telescope at Lick Observatory. The adaptive optics system is mounted on the bottom of the telescope at the Cassegrain focus, and the dye laser and beam projector is mounted on the side of the telescope.

a nominal stroke of 8 μm at 80 volts and less than 5% hysteresis. In the current configuration, 36 actuators are actively controlled; 25 are slaved, and 66 are kept fixed since they lie well outside the clear aperture of the telescope. The inter-actuator spacing is 11 mm at the deformable mirror corresponding to 46 cm mapped onto the telescope primary aperture.

The Lick adaptive optics system also contains a separate tip-tilt system for two reasons. First, it is needed to conserve the dynamic range of the deformable mirror. Second, when the wavefront information is obtained from a laser reference star, the tip-tilt information must be obtained separately from a natural star. The tip-tilt system is based on a set of four photon-counting avalanche photodiodes operated as a quad cell and a small (2.5 cm) tip-tilt mirror with an analog controller.

A picture of the Lick adaptive optics system is shown in Figure 2, and the optical layout is shown in Figure 3.

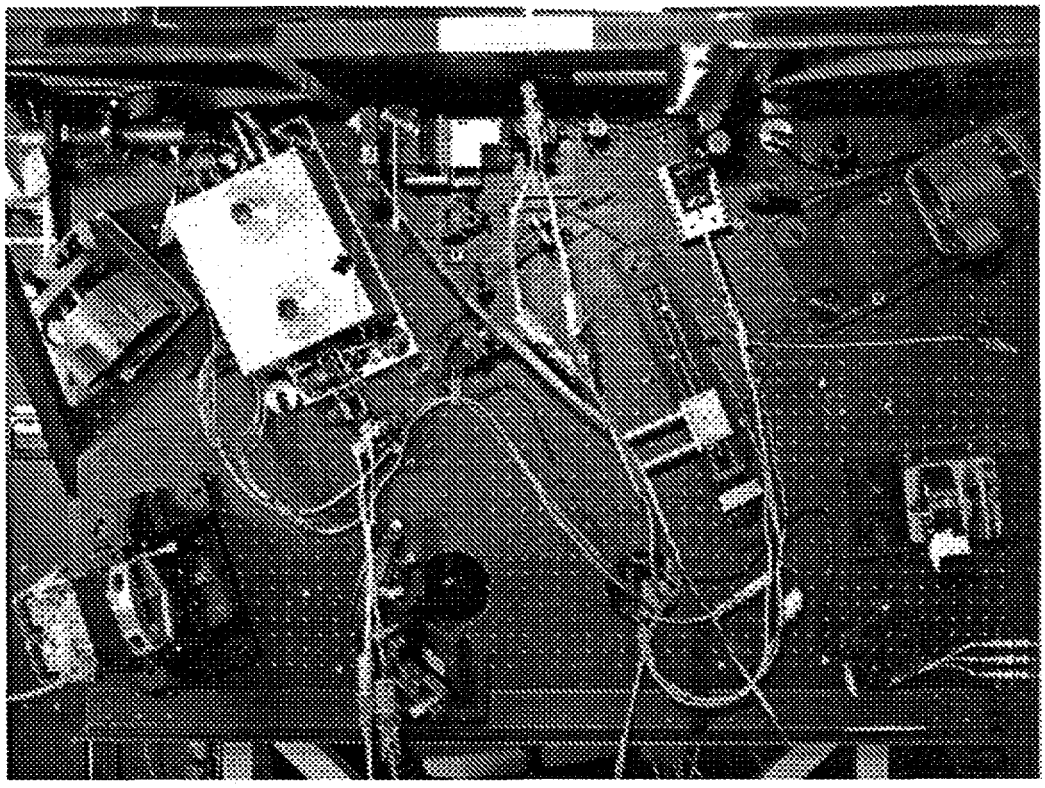

Figure 2 – Lick adaptive optics system. The wavefront sensor camera is contained in the large box on the upper left, and the deformable mirror is on the lower left. The imaging cameras and tip-tilt sensor are on the other side of the optical bench.

Light from the telescope enters from the top center on the diagram and hits two turning mirrors, the tip-tilt mirror, an off-axis parabolic collimating mirror, another turning mirror, and then the deformable mirror. The light then hits a dichroic beam splitter that reflects the light at $\lambda = 0.589$ μm ± 10 nm to the wavefront sensor leg that consists of an off-axis parabolic focusing mirror, a turning mirror, a collimating lens, the lenslet array, and finally the wavefront sensor camera.

The light not at $\lambda = 0.589$ μm ± 10 nm passes through the dichroic beam splitter to the science camera leg that consists of an off-axis focusing mirror, two turning mirrors that send the light to the other side of the optical bench, and a dichroic beam splitter that reflects the light at wavelengths longer than 1.0 μm to an infra-red science camera. The light at wavelengths shorter than 1.0 μm passes through the dichroic beam splitter to a beam splitter cube that sends half the light to the tip-tilt sensor and half the light to a CCD science camera and a CCD alignment and focusing camera.

2.2 Laser Guide Star System

The Lick laser guide star system uses a set of flash-lamp-pumped frequency-doubled solid-state (Nd-Yag) lasers to pump a dye laser. The pump lasers are located in a room below the floor of the Shane telescope dome and are fiber-optically coupled to a dye laser that is mounted on the south side of the Shane telescope. The dye laser produces light that can be tuned to the atomic sodium resonance line at 589 nm. The dye laser light is projected into the sky by a refractive launch telescope with a 30 cm primary lens that is also mounted on the south side of the Shane telescope. A more detailed description of the laser guide star system is given in another paper in this Proceedings[5].

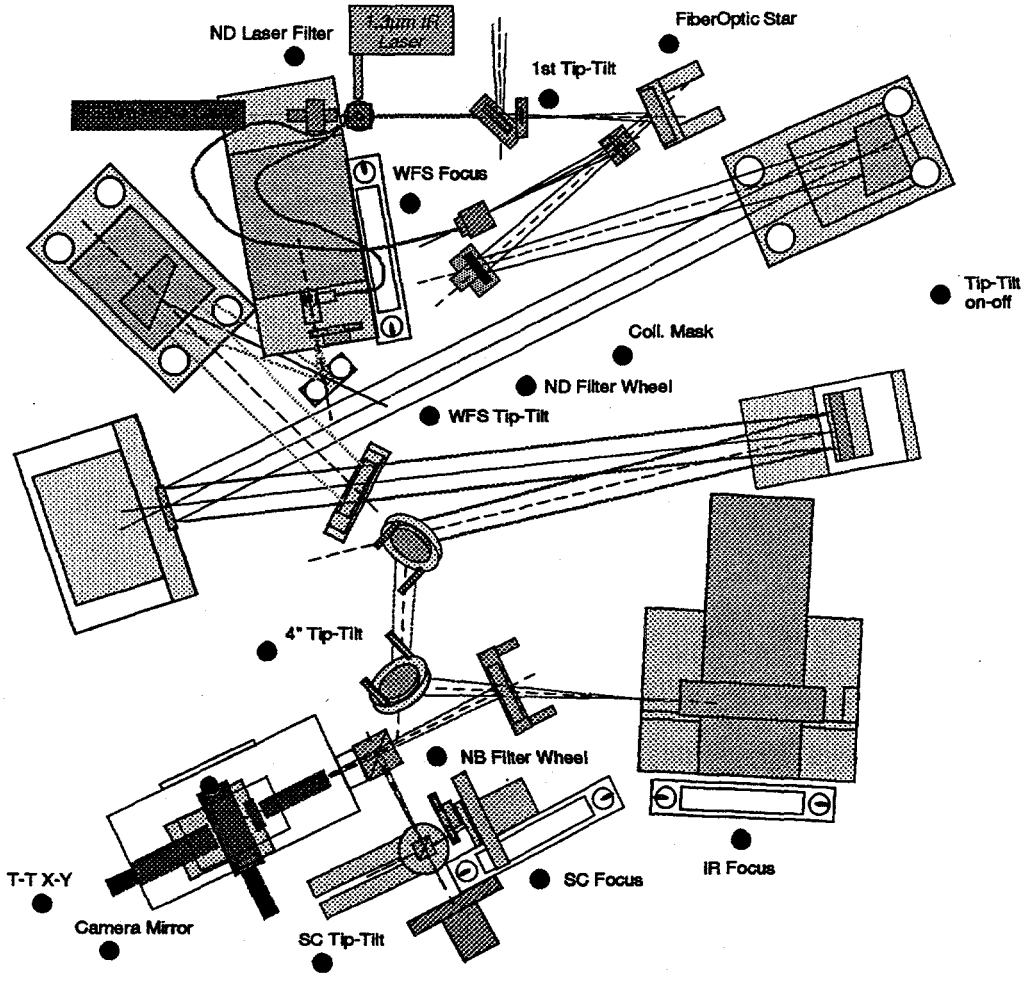

Figure 3 – Lick adaptive optics system layout.

3. ENGINEERING TEST RESULTS

3.1 Adaptive Optics System

An engineering test of the Lick adaptive optics system on the 3-meter Shane telescope was conducted on Oct. 25, 1994 using natural reference stars. The system configuration for this engineering test was similar to that described above except that a deformable mirror built by Itek for Lockheed with a rectangular array of 81 actuators (69 active and 12 slaved) was used in place of the 127-actuator LLNL deformable mirror which was still being assembled at the time. In addition, the wavefront sensor was configured with a rectangular array of 48 subapertures in the clear aperture of the telescope in order to match the geometry of the deformable mirror. Tests results for an earlier version of this system operating on the 1-meter Nickel telescope have been presented previously[6].

Radially averaged intensities for the open and closed-loop images of the star Alpha Perseus at a wavelength of 1.0 μm are shown in Figure 4. The images were taken with an exposure time of 100 seconds using a Photometrics CCD camera with a 1k $\times$ 1k Kodak chip. From the data shown in Figure 4, it is possible to calculate the FWHM

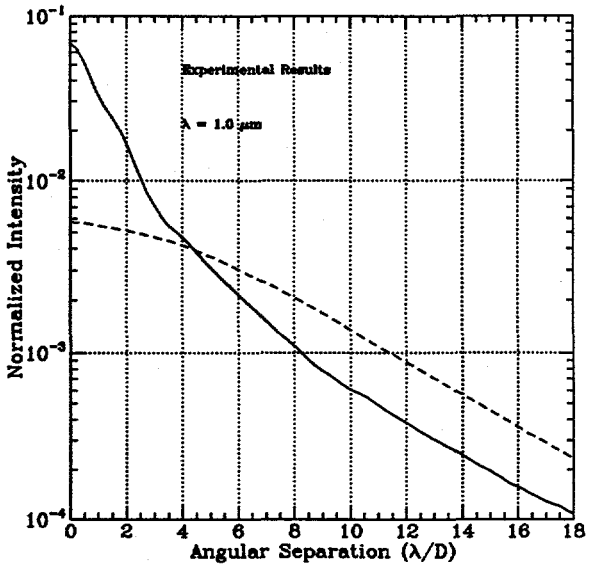

Figure 4 – Radially averaged image data from Alpha Perseus with and without adaptive optics compensation. These data were obtained during an engineering test of the Lick adaptive optics system on the 3-meter Shane telescope on Oct. 25, 1994.

of the images along with θ_{50} and θ_{80} (the angles that contain 50% and 80% of the light respectively). These values are given in Table 1a. The diffraction-limited FWHM is also given for comparison.

TABLE 1a. Alpha Perseus image angular statistics with and without adaptive optics compensation.

Data set	diff. lmtd. FWHM	FWHM	FWHM decrs.	incrs. from d. l.	θ_{50}	θ_{50} decrs.	θ_{80}	θ_{80} decrs.
1.0 μm								
open	0.069"	0.867"		12.6	1.16"		1.96"	
closed	0.069"	0.134"	6.5	1.9	0.58"	1.98	1.39"	1.41

The Strehl ratio of an image is defined as the ratio of the peak intensity of the image compared to the peak intensity of a diffraction-limited image that contains the same total amount of light. The Strehl ratios for the open and closed-loop images of Alpha Perseus have been calculated by direct comparison with simulated diffraction-limited images. This scaling has been applied in Figure 4, and the results for the Strehl ratios are given in Table 1b. The value of D/r_0 derived from the ratio of the open-loop to diffraction-limited FWHM, is also given in Table 1b. As theoretically expected, the open-loop Strehl ratio is approximately equal to $(D/r_0)^{-2}$.

TABLE 1b. Alpha Perseus image peak intensity statistics with and without adaptive optics compensation.

Data set	D/r_0	Strehl ratio	Strehl incrs.
1.0 μm			
open	12.6	0.00575	
closed	12.6	0.0674	11.7

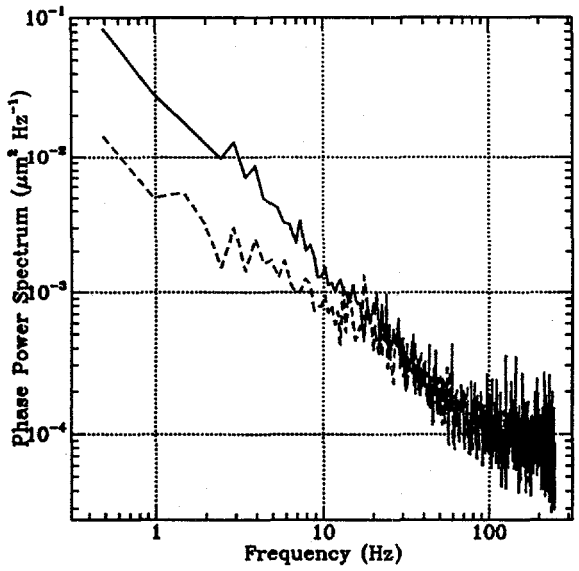

Figure 5 – Wavefront phase power spectra from Alpha Perseus with and without adaptive optics compensation. These data were obtained during an engineering test of the Lick adaptive optics system on the 3-meter Shane telescope on Oct. 25, 1994.

During this engineering test, time series of open and closed-loop wavefront tilt data were also collected for the star Alpha Perseus. These data were reconstructed to give wavefront phase, and then the Fourier transform was calculated for the time series of wavefront phase at each reconstruction position in the pupil. The results were then averaged for all reconstruction positions, and the resulting average phase power spectra are shown in Figure 5.

The frequency where the open and closed-loop power spectra cross is a measure of the system bandwidth. From these data, the system bandwidth is found to be $\sim$ 30 Hz, which is consistent with the analysis of the control system.[4]

In principle, the atmospheric coherence frequency can be derived from the phase power spectrum by integrating the power spectrum from infinite frequency back to that frequency where a total residual phase error of 1 rad^2 is obtained. The atmospheric coherence frequency found by this process can be used to compute the expected performance of the system under the assumption of Kolmogorov turbulence. However, inspection of the

data shown in Figure 5 reveals that the phase power spectrum is scaling with the -4/3 power of frequency compared to the -8/3 power predicted by Kolmogorov theory[7].

Since the scaling with frequency of the measured phase power spectrum is much different than that expected from Kolmogorov theory, a different method must be used to calculate the atmospheric coherence frequency for the purpose of computing expected performance. The method we will use here is to use equation (3) given below as the definition of the coherence frequency. Using the measured values of the control bandwidth and the residual servo error, which is the integral under phase power spectrum with adaptive optics correction, the atmospheric coherence frequency can be calculated. This has been done using the data in Figure 5 and assuming that the power spectrum is flat below 0.5 Hz and continues to scale with the -4/3 power of frequency above 100 Hz. The result is an atmospheric coherence frequency of 58 Hz at a wavelength of 1.0 μm.

3.2 Laser Guide Star System

The laser guide star system has been installed and operated on the telescope. A picture of the first propagation of the beam out of the dome is shown in Figure 6. The power output of the laser on the telescope has been measured to be over 20 W. A more detailed description of the engineering tests and results is given in another paper in this Proceedings[5].

4. COMPARISON TO THEORY

There are six main sources of error inherent in laser guide star adaptive optics compensation. Each of these errors is introduced because of a difference between the estimate of the reference wavefront and the actual wavefront of the astronomical object being imaged. To first order, we can treat the errors from each of the four sources as being uncorrelated. Therefore, the square of the residual wavefront phase error will be given by the quadrature sum:

$$\sigma_{\rm wf}^2 = \sigma_{\rm wfs}^2 + \sigma_{\rm dm}^2 + \sigma_{\rm servo}^2 + \sigma_{\rm aniso}^2 + \sigma_{\rm cone}^2 + \sigma_{\rm cal}^2. \quad (1)$$

where $\sigma_{\rm wfs}$ is the wavefront sensor measurement error, $\sigma_{\rm dm}$ is the deformable mirror fitting error, $\sigma_{\rm servo}$ is the servo bandwidth error, $\sigma_{\rm aniso}$ is the anisoplanatic error, $\sigma_{\rm cone}$ is the cone or focal anisoplanatic error, and $\sigma_{\rm cal}$ is the system calibration error.

The measurement error is due to the inability of the wavefront sensor to accurately measure the shape of the reference wavefront in the presence of noise. The fitting error is due to the inability of the deformable mirror to respond to the high-spatial-frequency variations of the atmosphere. The servo error is due to the inability of the control loop to respond to the high-temporal-frequency variations of the atmosphere. The anisoplanatic error is due to the difference in the atmospheric aberrations between the wavefront reference and the object being imaged. The cone error is due to the different cross-sections of the atmosphere that are sampled by the wavefront from the laser guide star located at a height of 100 km compared with the wavefront from a natural star. The calibration error is due to differences between the wavefront as measured by the wavefront sensor and the wavefront incident at the science camera.

Since the engineering test described in the previous section was conducted using a single bright natural star, the measurement, anisoplanatic, and cone errors were insignificant, so they will be neglected in this analysis.

The fitting error can be expressed as[8]

$$\sigma_{\rm dm}^2 = \mu(d/r_0)^{5/3}, \quad (2)$$

where d is the actuator spacing mapped to the entrance aperture of the telescope, and μ is a coefficient that depends on the deformable mirror geometry and influence function. For the ITEK mirror that was used, $\mu \approx 0.3$.

The servo error can be expressed as[7]

$$\sigma_{\rm servo}^2 = \beta(f_0/f_c)^{5/3} \quad (3)$$

where f_c is the servo closed-loop bandwidth defined as the frequency at which the spectrum of the control loop crosses the -3 dB point; f_0 is the atmospheric coherence frequency, and β is a coefficient that depends on the spectral shape of the control loop transfer function. For the control loop we are using, $\beta \approx 1.0$.

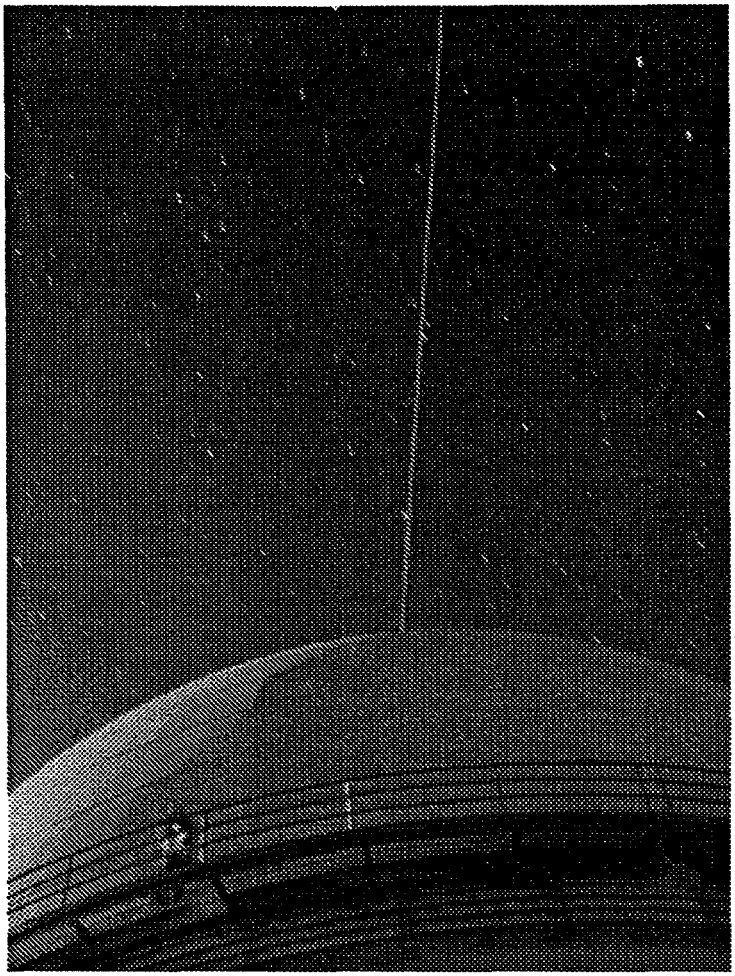

Figure 6 – First propagation of beam from Lick sodium-layer laser guide star system, April 1995.

In the limit of small phase error, the Strehl ratio due to the fitting error is given by

$$S_{\rm dm} = \exp(-\sigma^2_{\rm dm}) \tag{4}$$

The range over which equation (4) is a good approximation depends on the number of degrees of freedom controlled by the adaptive optics system[9]. For the case considered here, an adaptive optics system with $\sim$ 100 degrees of freedom, this formula is valid out to $\sigma^2_{\rm dm} \sim 7$ rad^2 (i.e., down to Strehl ratios of $\sim 10^{-3}$. This range is adequate for the analysis presented here.

The Strehl ratio due to the servo error depends on the value of D/r_0. An expression for the Strehl ratio due to servo error that includes the dependence on D/r_0 has been derived and numerically evaluated by Tyler[10]. Tyler's numerical results for the Strehl ratio due to servo error can be approximated by the expression

$$S_{\rm servo} = \exp\left[-F(D/r_0)\,\sigma^2_{\rm servo}\right], \tag{5}$$

where

$$F(D/r_0) \equiv [1 + 1/\log_{10}(D/r_0)]^{-5/3} . \quad (6)$$

Using equations (1)-(6) and the measured values of D/r_0, f_c, and f_0 it is possible to compute the expected value for the Strehl ratio of the image data presented in the previous section. This quantity is given in Table 2 along with the individual wavefront error terms and Strehl ratios including the measured value of the calibration error.

TABLE 2. Predicted error terms and Strehl ratio for Alpha Perseus image data after adaptive optics compensation.

Data set	σ^2_{dm} (rad^2)	σ^2_{servo} (rad^2)	σ^2_{cal} (rad^2)	S_{dm}	S_{servo}	S_{cal}	Strehl ratio
1.0 μm	0.64	3.0	0.56	0.53	0.37	0.57	0.11

By comparing the values in Table 1b and Table 2, it can be seen that the predicted Strehl ratio is a factor of 1.6 higher than the measured value. This is most likely due to the non-Kolmogorov nature of the measured phase power spectrum which will decrease the accuracy of the equations used in this section since they were all derived explicitly assuming Kolmogorov theory.

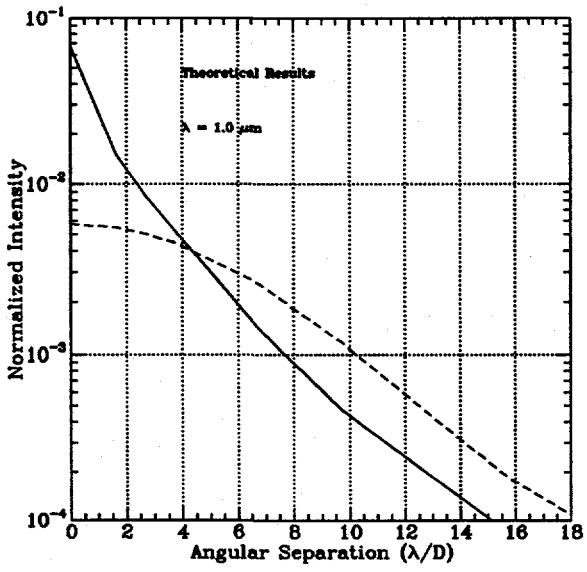

Figure 7 – Theoretical open and closed-loop PSFs using a spatial filter model for the adaptive optics system. The width of the spatial filter has been set so that the closed-loop results give the measured Strehl ratios. These theoretical PSFs are in good agreement with the measured PSFs shown in Figure 4.

A more detailed theoretical model of the Alpha Perseus imaging data can be constructed by modeling the adaptive optics system as a spatial filter on the wavefront phase spatial power spectrum.[9] This analysis allows one

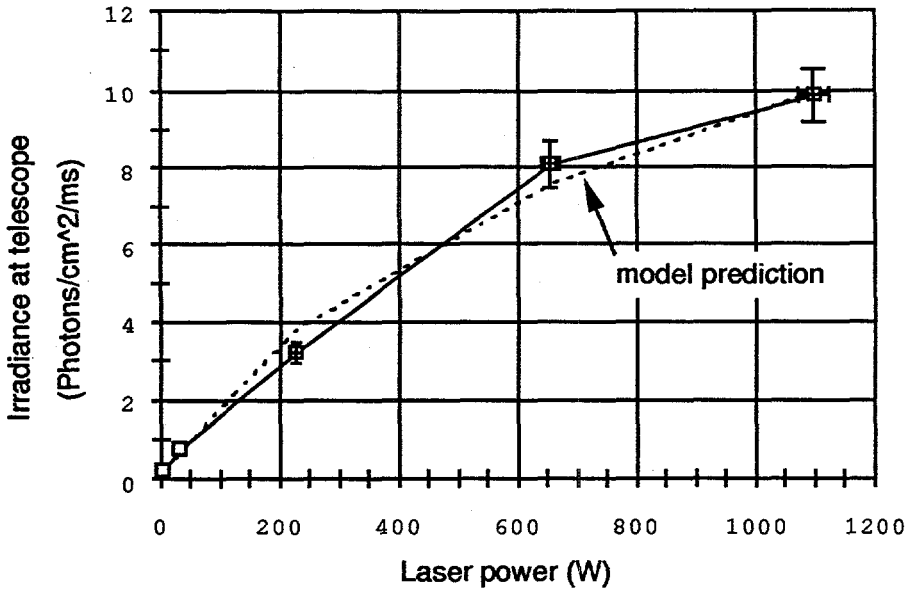

Figure 8 – Return flux as a function of laser power for a pulsed dye laser system operated at LLNL.

to compute the expected MTF and PSF for the system. Figure 7 shows the theoretical open and closed-loop PSFs calculated using the measured values of D/r_0. The width of the spatial filter was chosen to match the measured closed-loop Strehl ratio. Comparing Figures 7 and 4, it can be seen that there is good agreement in the details of the experimental and theoretical PSFs.

5. PERFORMANCE PREDICTIONS

Atmospheric seeing characteristics have been measured at Lick Observatory and results have been presented in a previous paper[6]. Median seeing at Lick observatory can be characterized at $\lambda = 0.55$ μm by $r_0 = 6$ cm, $f_0 = 170$ Hz and $\theta_0 = 3$ arc seconds. Good seeing at Lick observatory can be characterized at $\lambda = 0.55$ μm by $r_0 = 10$ cm, $f_0 = 100$ Hz and $\theta_0 = 5$ arc seconds.

Return flux from the sodium layer has been previously measured for a pulsed dye laser system at LLNL that was similar to the one now installed at Lick Observatory[11]. The data from these measurements is shown in Figure 8. Since the site of LLNL is less than 50 km from the site of Lick Observatory, this data should accurately reflect the return flux from the Lick laser guide star system. From Figure 8, it can be seen that the expected return flux for a 20 W laser system is 0.5 photons cm^{-2} ms^{-1}. This return flux is equivalent to a star of about 8th magnitude.

Using the measured values of the atmospheric parameters and the measured system parameters, it is possible to predict the performance of the integrated Lick laser guide star adaptive optics system on the 3-meter Shane telescope.

Figure 9 shows the expected performance of the Lick adaptive optics system on the 3-meter Shane telescope at 2.2 μm and with the different seeing conditions as a function of the magnitude of the reference star. For bright stars, the system will be limited by both the fitting and the servo error. For dimmer stars, the system is also limited by the measurement error. In this regime, servo bandwidth has been chosen to give the optimal relationship between servo error and measurement error.

The performance of the Lick adaptive optics system using the laser reference star shown in Figure 9 does not include the degradation from the cone effect. The magnitude of this effect can be calculated by $S_{\text{cone}} = \exp(-\sigma^2_{\text{cone}})$,

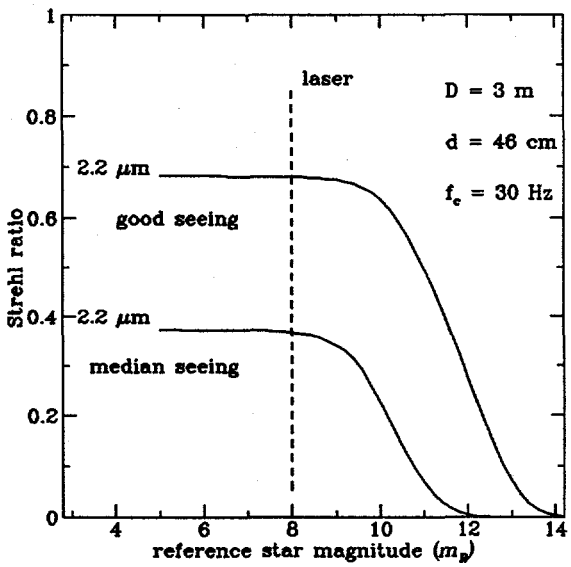

Figure 9 – Expected performance of the Lick adaptive optics system on the 3-meter Shane telescope. The dashed line marks the expected performance when the system is operated using the laser guide star.

where $\sigma^2_{\text{cone}} = (D/d_0)^{5/3}$.[12] The value of d_0 can be approximated by $2.5\theta_0 H$, where H is the height of the guide star[13]. Using these formulas, the Strehl degradation for $\lambda = 2.2$ μm can be shown to be $S_{\text{cone}} = 0.96$ for median seeing and $S_{\text{cone}} = 0.98$ for good seeing. Therefore, the cone effect is not expected to be significant for the cases under consideration, and the curves shown in Figure 9 can be taken to accurately represent the expected performance of the integrated Lick laser guide star adaptive optics system.

6. ACKNOWLEDGMENTS

Work performed under the auspices of the U.S. Department of Energy by Lawrence Livermore National Laboratory under Contract W-7405-Eng-48.

7. REFERENCES

1. H. W. Babcock, "Adaptive optics revisited," Science, **249**, 253-257 (1990).
2. W. Happer, G. MacDonald, C. E. Max, and F. Dyson, "Atmospheric-turbulence compensation by resonant optical backscattering from the sodium layer in the upper atmosphere," J. Opt. Soc. Am. A, **11**, 263-276 (1994).
3. L. A. Thompson, "Adaptive optics in astronomy," Physics Today, **47**, **12**, 24-31 (1994).
4. J. M. Brase, J. An, K. Avicola, H. D. Bissinger, H. W. Friedman, D. T. Gavel, B. Johnston, C. E. Max, S. S. Olivier, R. Presta, D. A. Rapp, J. T. Salmon, and K. E. Waltjen, "Adaptive optics at Lick Observatory: System architecture and operations," Proc. Soc. Photo-Opt. Instrum. Eng., **2201**, 474-488 (1994).
5. H. W. Friedman, G. V. Erbert, T. C. Kuklo, J. G. Malik, J. T. Salmon, D. A. Smauley, G. R. Thompson, and N. J. Wong, "Sodium beacon laser system for the Lick Observatory," Proc. Soc. Photo-Opt. Instrum. Eng., **2534**, in press (1995).
6. S. S. Olivier, J. An, K. Avicola, H. D. Bissinger, J. M. Brase, H. W. Friedman, D. T. Gavel, E. M. Johansson, C. E. Max, K. E. Waltjen, W. Fisher, and W. Bradford, "Performance of adaptive optics at Lick Observatory," Proc. Soc. Photo-Opt. Instrum. Eng., **2201**, 1110-1120 (1994).

7. D. P. Greenwood and D. L. Fried, "Power spectra requirements for wave-front-compensative systems," J. Opt. Soc. Am., **66**, 193-206 (1976).

8. D. L. Fried, "Statistics of a geometric representation of wavefront distortion," J. Opt. Soc. Am., **55**, 1427-1435 (1965).

9. D. T. Gavel and S. S. Olivier, "Simulation and analysis of laser guide star adaptive optics systems for the 8- to 10-meter-class telescopes," Proc. Soc. Photo-Opt. Instrum. Eng., **2201**, 295-303 (1994).

10. G. A. Tyler, "Turbulence-induced adaptive-optics performance degradation: evaluation in the time domain," J. Opt. Soc. Am. A, **1**, 251-262 (1984).

11. K. Avicola, J. M. Brase, J. R. Morris, H. D. Bissinger, J. M. Duff, H. W. Friedman, D. T. Gavel, C. E. Max, S. S. Olivier, R. W. Presta, D. A. Rapp, J. T. Salmon, and K. E. Waltjen, "Sodium-layer laser guide star experimental results," J. Opt. Soc. Am. A, **11**, 825-831 (1994).

12. D. Fried and J. F. Belsher, "Analysis of fundamental limits to artificial-guide-star adaptive-optics-system performance for astronomical imaging," J. Opt. Soc. Am. A, **11**, 227-287 (1994).

13. G. Tyler, "Rapid evaluation of d_0: the effective diameter of a laser-guide-star adaptive-optics system," J. Opt. Soc. Am. A, **11**, 325-338 (1994).